Systems/Circuits

The Neural Basis for Biased Behavioral Responses Evoked by Galvanic Vestibular Stimulation in Primates

Patrick A. Forbes,[1*] Annie Kwan,[2*] Diana E. Mitchell,[3] Jean-Sébastien Blouin,[4] and Kathleen E. Cullen[3,5,6,7,8]
[1]Department of Neuroscience, Erasmus MC, University Medical Center Rotterdam, 3000 CA Rotterdam, The Netherlands, [2]Departments of Biomedical Engineering and, [3]Physiology, McGill University, Montréal, Québec H3G 1Y6, Canada, [4]School of Kinesiology, University of British Columbia, Vancouver, British Colombia V6T 1Z1, Canada, [5]Departments of Biomedical Engineering, [6]Otolaryngology-Head and Neck Surgery, and, [7]Neuroscience, Johns Hopkins University, Baltimore, Maryland 21205, and [8]Kavli Neuroscience Discovery Institute, Johns Hopkins University, Baltimore, Maryland 21205

Noninvasive electrical stimulation of the vestibular system in humans has become an increasingly popular tool with a broad range of research and clinical applications. However, common assumptions regarding the neural mechanisms that underlie the activation of central vestibular pathways through such stimulation, known as galvanic vestibular stimulation (GVS), have not been directly tested. Here, we show that GVS is encoded by VIIIth nerve vestibular afferents with nonlinear dynamics that differ markedly from those predicted by current models. GVS produced asymmetric activation of both semicircular canal and otolith afferents to the onset versus offset and cathode versus anode of applied current, that in turn produced asymmetric eye movement responses in three awake-behaving male monkeys. Additionally, using computational methods, we demonstrate that the experimentally observed nonlinear neural response dynamics lead to an unexpected directional bias in the net population response when the information from both vestibular nerves is centrally integrated. Together our findings reveal the neural basis by which GVS activates the vestibular system, establish that neural response dynamics differ markedly from current predictions, and advance our mechanistic understanding of how asymmetric activation of the peripheral vestibular system alters vestibular function. We suggest that such nonlinear encoding is a general feature of neural processing that will be common across different noninvasive electrical stimulation approaches.

Key words: **asymmetry; galvanic vestibular stimulation; modeling; nonlinear; vestibular afferent**

Significance Statement

Here, we show that the application of noninvasive electrical currents to the vestibular system (GVS) induces more complex responses than commonly assumed. We recorded vestibular afferent activity in macaque monkeys exposed to GVS using a setup analogous to human studies. GVS evoked notable asymmetries in irregular afferent responses to cathodal versus anodal currents. We developed a nonlinear model explaining these GVS-evoked afferent responses. Our model predicts that GVS induces directional biases in centrally integrated head motion signals and establishes electrical stimuli that recreate physiologically plausible sensations of motion. Altogether, our findings provide new insights into how GVS activates the vestibular system, which will be vital to advancing new clinical and biomedical applications.

Introduction

Vestibular sensory signals encode head movement and orientation in space to shape our actions and perception in everyday life as we move and interact within our environment. During such self-motion, the vestibular system is inevitably activated in concert with other sensory modalities (e.g., vision, proprioception). As such, studying the vestibular system requires techniques that allow for independent investigation from other sources of sensory feedback. A promising approach to target and understand the functional role of the vestibular system is the application of localized currents via surface electrodes placed bilaterally behind the ears on the mastoid process (Fitzpatrick and Day, 2004; Forbes et al., 2015; Dlugaiczyk et al., 2019). This noninvasive

Received May 23, 2022; revised Jan. 25, 2023; accepted Jan. 30, 2023.
Author contributions: P.A.F., A.K., J.-S.B., and K.E.C. designed research; P.A.F., A.K., and D.E.M. performed research; P.A.F. and A.K. analyzed data; and P.A.F., A.K., J.-S.B., and K.E.C. wrote the paper.
This work was supported by National Institutes of Health–National Institute on Deafness and Other Communication Disorders Grants R01-DC002390, R01-DC013069, and 1UF1NS111695 to K.E.C. P.A.F. was supported by Dutch Research Council Grants 016.Veni.188.049 and VI.Vidi.203.066, and J.-S.B. was supported by Natural Sciences and Engineering Research Council of Canada Grant RGPIN-2020-05438. We thank Maurice Chacron for critical feedback on the manuscript.
*P.A.F. and A.K. contributed equally to this work.
The authors declare no competing financial interests.
Correspondence should be addressed to Kathleen E. Cullen at kathleen.cullen@jhu.edu.
https://doi.org/10.1523/JNEUROSCI.0987-22.2023

technique, known as galvanic vestibular stimulation (GVS), is unique in that it activates the vestibular sensory organs in absence of actual head movement. Given this advantageous property, GVS has become a fundamental tool for advancing our understanding of specific contributions of the vestibular system to the control of gaze, balance, locomotion, and perception (Britton et al., 1993; Day et al., 1997; Zink et al., 1998; Schneider et al., 2002; Wardman et al., 2003b; Fitzpatrick et al., 2006; Forbes et al., 2016; 2017; Chen et al., 2019; Khosravi-Hashemi et al., 2019; Dietrich et al., 2020). Additionally, GVS has emerged as a tool for clinically assessing and treating vestibular and other neurologic disorders (Kim et al., 2006; Aw et al., 2013; Bunn et al., 2015; Schniepp et al., 2018; Woll et al., 2019). However, despite its popularity, how GVS actually activates vestibular pathways to give rise to behavioral responses and self-motion perception is unknown.

Conventional wisdom is that the activation of the vestibular system through the external application of GVS is inherently linear. Implicit to this view is the assumption that stimulation with symmetrical currents of opposite polarity will give rise to symmetrical virtual sensations of self-motion (Fitzpatrick and Day, 2004; St George et al., 2011). This assumption has critical implications for how GVS can be effectively leveraged to study vestibular function and treat neurologic disorders. In support of this view, reports based on human behavioral studies largely emphasize symmetry in ocular, balance, and navigation responses evoked by GVS (Day et al., 1997; Zink et al., 1998; Jahn et al., 2003a; Bent et al., 2004; Mian and Day, 2009), leading some investigators to combine evoked responses from stimuli of opposite polarity to improve signal-to-noise ratios (Day et al., 1997; Cathers et al., 2005; Mian and Day, 2014; Fitzpatrick and Watson, 2015; Mackenzie and Reynolds, 2018; Magnani et al., 2021). However, this view is at odds with results obtained in rodent models showing that vestibular afferents are asymmetrically activated when currents of opposing polarities are applied within the inner ear (i.e., in much closer proximity to the vestibular end organs compared with external GVS; Kim and Curthoys, 2004; Manca et al., 2019).

Here, we used our nonhuman primate model for transmastoid GVS (Kwan et al., 2019) to explicitly investigate the linearity of the neural mechanisms underlying the activation of vestibular pathways. We found that the assumption of linearity is not valid. Instead, vestibular afferents displayed asymmetric responses to currents of opposing polarities. These asymmetries, which were marked in both the semicircular canal and otolith systems, in turn lead to comparable asymmetries in resultant oculomotor responses. Importantly, the dynamics of afferent activation differed markedly from those predicted by current models (Kwan et al., 2019), indicating that the time-varying GVS currents required to induce virtual sensations of constant head acceleration are distinct from those that are currently used. Finally, using computational modeling, we demonstrate that the nonlinear effect of GVS revealed by our experimental findings unexpectedly leads to a directional bias in the net population response when the information from both vestibular nerves is centrally integrated. Together our findings have important consequences for understanding the neural representation of GVS in central pathways; they provide insight into the general question of how noninvasive electrical stimulation of the brain activates neural pathways that generate perception and behavior, and make explicit predictions for future clinical and biomedical studies.

Materials and Methods

Three male macaque monkeys (two *Macaca fascicularis*, monkeys B and H; one *Macaca mulatta*, monkey D) were prepared for chronic extracellular recording using aseptic surgical techniques. All experimental protocols were approved by the McGill University Animal Care Committee and were in compliance with the guidelines of the Canadian Council on Animal Care.

Surgical procedures. The surgical preparation for monkeys B and D followed the procedures described previously (Dale and Cullen, 2013). The surgical preparation for monkey H followed new protocol procedures described in Kwan et al. (2019). Briefly, in all animals, aseptic surgical techniques were used, and under isoflurane anesthesia (0.8–1.5%), we secured a stainless steel post to the skull of the animal with stainless steel screws and dental acrylic, permitting complete immobilization of the head of the animal during the experiments, and implanted a chamber for chronic extracellular recording. Postsurgery protocol for monkeys B and D followed that described previously (Dale and Cullen, 2013); for monkey H, the procedures are detailed in Kwan et al. (2019). Animals were given at least 2 weeks to recuperate from the surgery before any experiments began.

Data acquisition. During the experiments, monkeys were head restrained and seated comfortably in a primate chair mounted on top of a vestibular turntable. Three-dimensional eye positions were measured using a modified eye tracker (Chronos Vision) fixed onto the head post of the monkey. Off-line analysis software Iris (Chronos Vision) was later used to calculate torsional eye position from markers applied near the limbus. Markers consisted of an infrared absorbing cosmetic pigment, Eisenoixid 316/Schwarz (Carl Jäger Tonindustriebedarf), dissolved in distilled water and applied near the limbus using a sterile surgical marking pen.

The left vestibular nerve was found as described in Jamali et al. (2013). Extracellular single-unit activity of primary vestibular afferents (semicircular canal and otolith) was recorded using tungsten microelectrodes (7–10 MΩ and 20–25 MΩ, Frederick-Haer). Neural signals were bandpass filtered from 300 to 3 kHz and sampled at 30 kHz. Head linear acceleration and angular velocity was measured by a three-dimensional linear accelerometer (Analog Devices) and a one-dimensional angular gyroscope (Watson), respectively, both firmly secured to the head post of the animal. Head linear acceleration, head angular velocity, and galvanic vestibular stimulation signals were low-pass filtered at 250 Hz (eight-pole Bessel filter) and sampled at 1 kHz. Neural behavioral and stimulation data were collected through the Cerebus Neural Signal Processor (Blackrock Microsystems). Neural data were imported into either Offline Sorter software (Plexon) as previously described (Dale and Cullen, 2015) or into a custom-written algorithm in MATLAB (MathWorks) to extract action potentials.

Experimental paradigms. For eye movement recordings, animals were placed in the dark while exposed to a sequence of 30 consecutive constant cathodal current GVS pulse stimulation of 1 mA lasting 40 s followed by a 20 s off period. Monkeys fixated on a centrally located laser target to minimize drift of the eye in horizontal and vertical directions. Rightward horizontal, upward vertical, and clockwise torsional (i.e., toward the right ear) eye movements are expressed as positive values. For neural recordings, once a unit was isolated, the vestibular end organs innervated by that fiber were determined based on the responses of the afferent to rotations or translation. Animals were then exposed to two different electrical stimuli. The first stimulation consisted of a repeated sequence of three consecutive constant cathodal or anodal current pulses of 1 mA lasting 40 s followed by a 20 s off period. The cathodal and anodal pulses were delivered in separate trials. The second stimulation consisted of a broadband Gaussian stochastic (0–25 Hz) current of maximum peak amplitude of 1 mA.

Galvanic vestibular stimuli were applied to animals using carbon rubber electrodes (~6 cm^2) in a binaural bipolar configuration. The electrodes were coated with Spectra 360 electrode gel (Parker Laboratories) and secured over the mastoid processes of the animal with a small bandage. The stimuli were generated using MATLAB and were delivered as analog signals to a constant current isolation unit (STMISOLA; Biopac

Systems) via a QNX-based real-time data acquisition system (Hays et al., 1982) or an arbitrary waveform generator (Keysight). The current polarity of the stimulation is referred relative to the polarity of the left stimulating electrode, which was on the same side of the vestibular afferents recorded.

Data analysis. All data were imported into MATLAB for analysis using custom-written algorithms. Eye position signals were digitally low-pass filtered with zero phase at 125 Hz using a 51st-order finite-impulse-response filter with a Hamming window. Segments of eye movements (horizontal, vertical, and torsional position) without saccades were first chosen over at least 20 trials, and slow phase velocity was computed from these segments.

Afferents were classified based on the regularity of resting discharge, which was evaluated by the normalized coefficient of variation (CV*), as done previously (Goldberg et al., 1984; Massot et al., 2011). Afferents with CV* $\leq$ 0.1 were considered regular, whereas those with CV* $>$ 0.1 were considered irregular (Sadeghi et al., 2009). The resting discharge of the afferents, in absence of electrical stimulation, was also computed. To estimate the time-dependent firing rate, FR(t), we first assigned the spike (spk) train R(t) as the binary sequence of action potentials with a bin width of 1 ms and then convolved the R(t) with a Gaussian (SD = 50 ms). We used a Gaussian probability density function to represent firing rates to prevent the introduction of localization error and/or nonlinearities (Richmond and Optican, 1990; Paulin, 1992).

For each afferent, responses to the constant current pulse were normalized by removing the baseline firing rate calculated 2 s before the onset of the stimulation and then averaged across the three pulses. We then characterized the afferent responses to the current pulses into three phases, onset (the maximum or minimum response within the first half second after at the start of cathodal or anodal current stimulation, respectively), steady-state (the mean responses within the last 5 s of the stimulation), and offset (the minimum or maximum responses relative to steady-state within the first half second after the cathodal or anodal current stimulation was turned off, respectively). To facilitate comparison across the three phases, we took the absolute values of these computed neural responses. To then assess the asymmetry of afferent responses to the constant current stimuli, an onset-offset asymmetry index was computed as the difference between the peak absolute responses at onset and offset. Comparable cathode-anode asymmetry indices were likewise used to assess the influence of stimulus polarity by computing the difference between peak responses during cathodal and anodal stimuli at the onset, steady-state, and offset phases of stimulation.

For each afferent, responses to the stochastic GVS of at least 30 s were used to estimate the transfer function using the following:

$$H(f) = P_{sr}(f)/P_{ss}(f), \tag{1}$$

where $P_{sr}(f)$ is the cross-spectrum between the stochastic stimulation and the spike train, and $P_{ss}(f)$ is the power spectrum of the stochastic stimulation. The gain and phase were then estimated from the transfer function. All spectral quantities were estimated using multitaper techniques with 32 Slepian functions (Jarvis and Mitra, 2001).

To better understand responses to sinusoidal GVS, we reanalyzed the data from Kwan et al. (2019) separately considering responses to cathodal versus anodal stimulation. Specifically, for each afferent a least-squares regression analysis was performed to determine the sensitivity of the cathodal and anodal cycle of the sinusoidal GVS according to the following equation:

$$FR(t) = gain \times GVS(t + \theta) + bias, \tag{2}$$

where $FR(t)$ is firing rate, *gain* is the afferent sensitivity to the sinusoidal GVS, θ is the phase shift relative to the GVS waveform, and *bias* is an offset representing resting discharge. Here, separate sensitivities for each portion of the cycle (cathodal and anodal) were fit simultaneously while maintaining a single bias and frequency-dependent phase shift. To then characterize the response dynamics of the afferent modulation resulting from GVS of opposing polarity, we estimated fractional order transfer functions described previously (Kwan et al., 2019) for each afferent type for responses produced by the entire stimulus as well as the cathodal and anodal cycles of the stimulus as follows:

$$H(f) = k\frac{s^{k_1}(1+bs)^{k_2}}{(1+as)}, \tag{3}$$

where $s = i2\pi f$, k is a gain factor, s^{k_1} is a frequency-independent adaptation operator, and $(1+as)$ and $(1+bs)^{k_2}$ are together responsible for high-frequency ($>$2–4 Hz) gain increase and phase leads. Parameter values were estimated from the population-averaged frequency responses to sinusoidal GVS using a least-squares regression to minimize the difference between the estimated and measured transfer functions in the complex form. The model receives as input the GVS signal and estimates as output the afferent firing rates. We then constructed a nonlinear model that combined the transfer functions of afferent responses to cathodal (H_c) and anodal (H_a) sinusoidal stimulation to predict the asymmetric afferent responses to constant current stimulation for each of the four afferent types (i.e., irregular vs regular canal and otolith afferents). We note that these models provide a mathematical representation of afferent firing rate dynamics and do not represent the physiological mechanisms involved in their evoked activity.

To estimate the virtual sensations of motion encoded by afferent firing produced by the cathodal versus anodal constant current stimulation, we inverted well-established linear models of afferent responses to actual motion (Goldberg et al., 2012; Schneider et al., 2015). Specifically, for canal afferents the model is given by the following transfer function consisting of two poles and two zeros:

$$H(f) = k\frac{s\left(s+\frac{1}{\tau_1}\right)}{\left(s+\frac{1}{\tau_c}\right)\left(s+\frac{1}{\tau_2}\right)}. \tag{4}$$

For regular canal afferents, parameter values were based on Schneider et al. (2015) as follows: k = 2.83 (spikes/s)/(degrees/s), τ_1 = 0.0175 s, τ_2 = 0.0027 s, and τ_c = 5.7 s. For irregular canal afferents, parameter values were as follows: k = 27.09 (spikes/s)/(degrees/s), τ_1 = 0.03 s, τ_2 = 0.0006 s, and τ_c = 5.7 s. For otolith afferents we used the same fractional order transfer function as implemented for the GVS stimulus (Eq. 3) but with parameters based on Schneider et al. (2015), k = 59.0106 (spikes/s)/G, k_1 = 0.0643, k_2 = 2.208, a = 0.0138 s, and b = 0.0255 s for regular afferents, and k = 112.7417 (spikes/s)/G, k_1 = 0.3084, k_2 = 2.6834, a = 0.0136 s, and b = 0.0318 s for irregular afferents. We note that these parameter values are similar to those used previously to best match available experimental data (canals, Hullar et al., 2005; Ramachandran and Lisberger, 2006; Sadeghi et al., 2007b; otoliths, Angelaki and Dickman, 2000; Jamali et al., 2013). Afferent firing rates recorded during the square wave GVS stimulation in this study were used as input to these (inverted) models to provide as output an estimate of the virtual signal of motion. Further, cathode-anode asymmetry indices similar to those described above for afferent firing rates were computed from these motion equivalent responses at the onset, steady-state, and offset phases of stimulation.

Finally, we estimated the net head motion signal produced by the combined activity of semicircular afferents to determine how GVS-evoked asymmetries influence the evoked sensations of head motion. We focused on semicircular canal response because near cancellation is predicted for the otolith end organs because of the mapping of response direction across the macula (Tribukait and Rosenhall, 2001; Fitzpatrick and Day, 2004). To compute the net head motion signal for input cathodal and anodal square wave GVS, we (1) used the cathodal and anodal GVS transfer functions (H_c and H_a, respectively) to estimate the predicted afferent firing rates from square wave GVS, and (2) we used the inverted models of afferent firing rate responses to actual motion (Schneider et al., 2015) to estimate the virtual rotational signals. To compute the signal provided by each specific semicircular canal, we ran simulations that assumed (1) input from only irregular afferents, (2) input from only regular afferents and (3) a 3:1 regular-to-irregular weighting

(Chen et al., 2022) based on afferent population distributions in the VIIIth cranial nerve (Baird et al., 1988; Goldberg, 2000). We then averaged the virtual rotational signals from the left and right side to compute the net signal from each canal pair [i.e., left horizontal-right horizontal, left anterior-right posterior (LARP), and right anterior-left posterior (RALP)]. Using the known anatomic orientations of the canals relative to Reid's stereotactic line (Della Santina et al., 2005), we projected the responses from each canal pair, together with the total signal of head motion, onto Cartesian coordinates in Reid's plane to generate virtual head motion signals in roll, pitch, and yaw.

Statistical analysis. Our sample sizes were similar to those generally used in the field (Sadeghi et al., 2007a; Jamali et al., 2013). Statistical analysis was performed in IBM SPSS Statistics software and Microsoft Excel. Statistical significance was set at $p < 0.05$. Before statistical analysis, normality of distributions was evaluated using a Shapiro-Wilk's test. To analyze the asymmetry in eye movement velocity between the onset and offset of the stimulus, we performed a two-tailed Student's *t* test within each monkey. A similar test was performed to assess the eye movement velocity between the onset and steady-state responses. To assess the dynamics of afferent responses to cathodal current GVS for canal and otolith afferents, two-tailed Student's *t* tests were used to compare regular versus irregular afferents at each stimulus phase (i.e., onset, steady-state, offset, and onset-offset difference) with a Bonferroni correction for multiple comparisons. To assess asymmetry between the onset and offset phases for each afferent type, a one-sample two-tailed Student's *t* test with a Bonferroni correction for multiple comparisons was also used to assess whether the onset-offset asymmetry index was different from zero.

To assess the dynamics of afferent responses to cathodal and anodal current GVS for canal and otolith afferents, two-tailed Student's *t* tests were again used to compare regular versus irregular afferents at each stimulus phase (i.e., onset, steady-state, offset) with a Bonferroni correction for multiple comparisons. To assess whether the cathode-anode asymmetry index was different from zero, a one-sample two-tailed Student's *t* test with a Bonferroni correction for multiple comparisons was also used. A similar analysis was also performed on the cathode-anode asymmetry index computed from the signals of motion equivalence estimated from the afferent firing rates.

To compare the responses to sinusoidal and stochastic stimulation, a Student's *t* test was conducted at each frequency, excluding 0.1 Hz, because that was not estimated in the stochastic response. In addition, differences in gain between anodal and cathodal phases of sinusoidal stimulation at each frequency were assessed using a linear mixed model (fixed effects, frequency and stimulus polarity; random effects, afferent number). The *p* value was corrected for multiple comparison using Bonferroni's corrections. All values are expressed as mean ± SEM unless otherwise stated.

Results

Asymmetric afferent responses evoked by the onset versus offset of cathodal GVS

To establish the neural basis of GVS-evoked responses we recorded from individual semicircular canal and otolith afferents (in the left VIIIth cranial nerve) of macaque monkeys. Afferents were first classified as regular or irregular (see above, Materials and Methods) based on their resting firing rate regularity in the absence of vestibular stimulation (Fig. 1*A*; for review, see Cullen, 2019). Our dataset consisted of $N = 67$ semicircular canal afferents, of which $N = 37$ were regular (mean CV* = 0.06 ± 0.00) and $N = 33$ were irregular (mean CV* = 0.40 ± 0.03). Mean resting discharge rates were 106.1 ± 3.7 spk s^{-1} and 90.6 ± 6.1 spk s^{-1}, respectively. The remaining $N = 43$ afferents were otolith afferents, of which $N = 20$ were regular (mean CV* = 0.05 ± 0.00) and $N = 23$ were irregular (mean CV* = 0.39 ± 0.02). Mean resting discharge rates were 73.3 ± 7.1 spk s^{-1} and 57.7 ± 5.0 spk s^{-1}, respectively.

To directly replicate the approach typically used for fundamental and clinical studies in humans, we applied GVS through surface electrodes that were placed behind the ears in a binaural bipolar configuration (Fitzpatrick and Day, 2004; Forbes et al., 2015; Dlugaiczyk et al., 2019). We first recorded the responses of individual afferents to standard cathodal step currents (Nashner and Wolfson, 1974; Britton et al., 1993; Day et al., 1997; Watson et al., 1998; Zink et al., 1998; Schneider et al., 2002; Wardman et al., 2003b; Fitzpatrick et al., 2006; Kim et al., 2006; Aw et al., 2013; Bunn et al., 2015). Irregular canal and otolith afferents (Fig. 1*B*,*C*) were strongly modulated by cathodal GVS (red traces, $N = 33$, $N = 23$) demonstrating (1) an initial, large transient excitatory response at stimulation onset, (2) a subsequent sustained steady-state response, and (3) a large inhibitory transient response at stimulation offset. In comparison, regular afferents (Fig. 1*B*,*C*) displayed weaker modulation throughout the duration of the same GVS stimulation (blue traces, $N = 37$, $N = 20$).

Figure 1, *D*–*G*, quantifies these findings for our populations of semicircular canal and otolith afferents (see above, Materials and Methods). Overall, responses were comparable for semicircular canal and otolith afferents, with irregular afferents displaying substantially stronger modulation relative to their regular counterparts (Fig. 1*D*–*F*; Student's *t* tests for each phase, $p < 0.017$, Bonferroni correction for multiple comparisons). The initial transient afferent responses decreased rapidly to reach a reduced steady-state response (compare Fig. 1*D*,*E*). Furthermore, stimulation onset evoked stronger transient responses than stimulation offset (Fig. 1*D* vs *F*; note, all responses are presented as absolute values). To emphasize this difference, we computed an onset-offset asymmetry index (Fig. 1*F*; see above, Materials and Methods), which was significantly different from zero for irregular afferents and regular canal afferents (Student's *t* tests, $p < 0.001$) but not regular otolith afferents (Student's *t* test, $p = 0.191$). Thus, irregular afferents, in both the semicircular canal and otolith systems, as well as regular canal afferents, demonstrated significantly asymmetric modulation in response to GVS step onset versus offset.

Asymmetric torsional eye movements evoked by the onset versus offset of cathodal GVS

The results presented above demonstrate that GVS activation of the vestibular nerve using standard cathodal step currents in a standard binaural bipolar configuration induces a significant response onset-offset asymmetry. Given that GVS evokes eye movements (Schneider et al., 2002; Aw et al., 2013; Chiarovano et al., 2015), we quantified the eye movements evoked by the same GVS stimulus in our monkey model. As can be seen in Figure 2*B*, stimulation induced a transient predominately torsional eye movement in the clockwise direction. This eye movement rapidly decayed to reach a substantially lower steady-state velocity within the 40 s stimulation period, and the offset of stimulation then induced a transient torsional eye movement in the opposite direction (counterclockwise). Figure 2*C* quantifies the predicted asymmetry with transient eye velocity responses to GVS offset being significantly less than its onset (Fig. 2*C*; monkey D, $p = 0.01$, $t_{(15)} = 2.9$; monkey B, $p = 0.004$, $t_{(17)} = 3.4$; monkey S, $p = 0.008$, $t_{(5)} = 4.3$). To emphasize this difference, we again computed an onset-offset asymmetry index, which was significantly different for all monkeys (Fig. 2*D*). In contrast, in the horizontal and vertical directions, GVS induced smaller eye movements (Fig. 1*B*) with nearly no significant asymmetry for

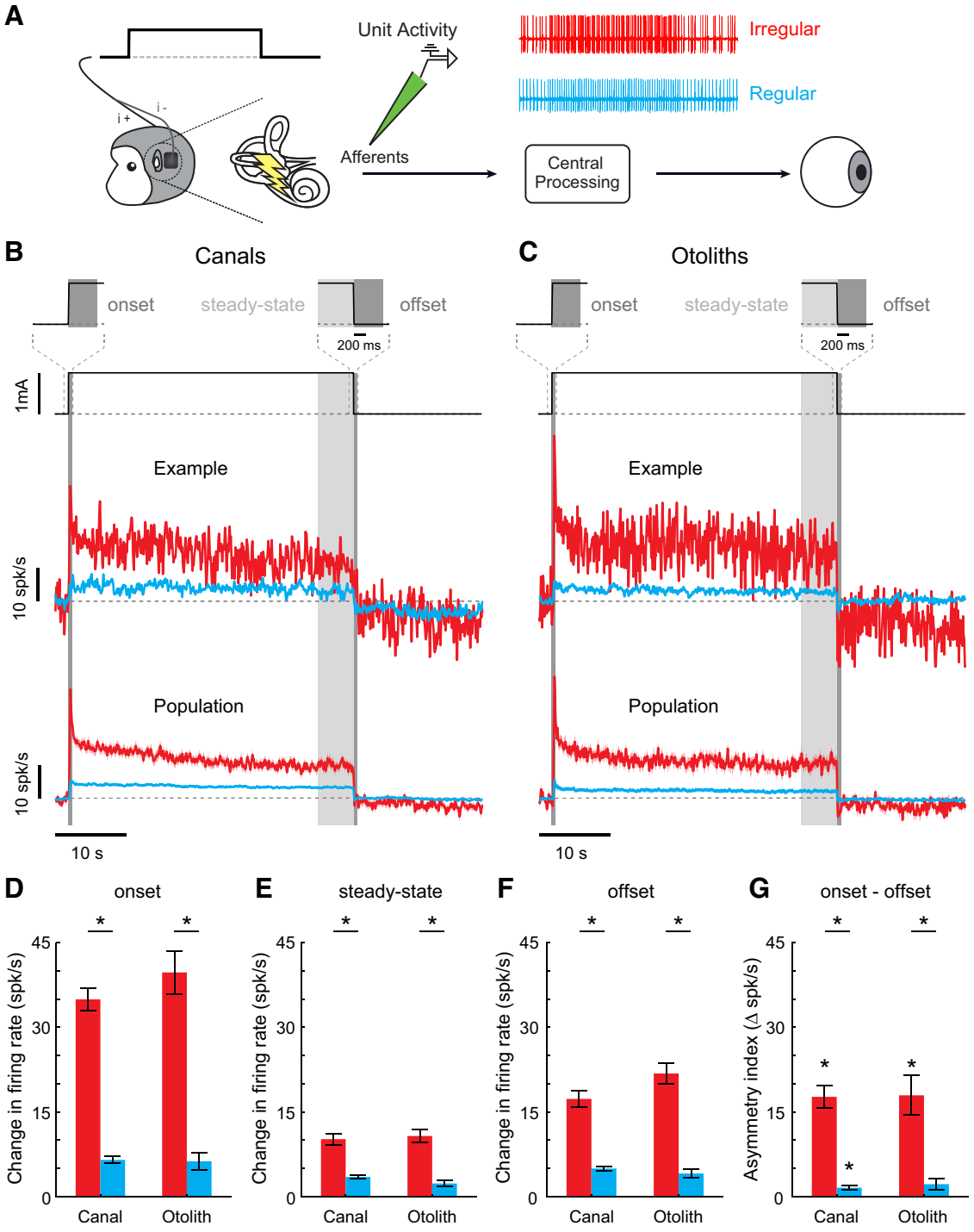

Figure 1. Constant cathodal current GVS evokes asymmetric changes in afferent firing rates at stimulus onset versus offset. ***A***, We recorded extracellular single-unit activity from regular and irregular vestibular afferents using tungsten electrodes during constant cathodal current GVS. ***B***, Top row, Constant cathodal current GVS. Middle row, Average firing rate across three constant current pulses of example regular (blue) and irregular (red) canal afferents relative to a 2 s baseline before the onset of the stimulation. Bottom row, The population averaged responses of the regular ($N = 37$) and irregular ($N = 33$) canal afferents to the cathodal current, which depicts an initial transient increase in firing rate, a subsequent steady-state response, and a transient decrease in firing rate. ***C***, Top row, Constant cathodal current GVS. Middle row, Average firing rate across three constant current pulses of example regular (blue) and irregular (red) otolith afferents relative to a 2 s baseline before the onset of the stimulation. Bottom row, The population averaged responses of the regular ($N = 20$) and irregular ($N = 23$) otolith afferents to the cathodal current with similar characteristics as observed in canal afferents. For ***B*** and ***C***, afferent firing rates were normalized by removing the baseline firing rate calculated 2 s before the onset of the stimulation and therefore varied relative to 0 spks/s (i.e., horizontal dashed line). ***D***, The population average peak change in firing rate (absolute value) within the first 0.5 s after the onset of the stimulation for the different classes of vestibular afferents. ***E***, The population average steady-state response (absolute value) within the last 5 s of the stimulation. ***F***, The population average peak change in firing rate (absolute value) within the first 0.5 s after the offset of the stimulation relative to the preceding steady-state firing rate. ***G***, The population average onset-offset asymmetry index (i.e., peak onset minus peak offset) was significantly different from zero ($p < 0.001$) for all afferents except regular otoliths ($p = 0.191$). For all four measures, there was a significant difference in response between the discharge regularity of the afferents (irregular vs regular; $p < 0.017$). Error bars and shaded regions indicate the SEM. Asterisks indicate significant differences for the compared responses.

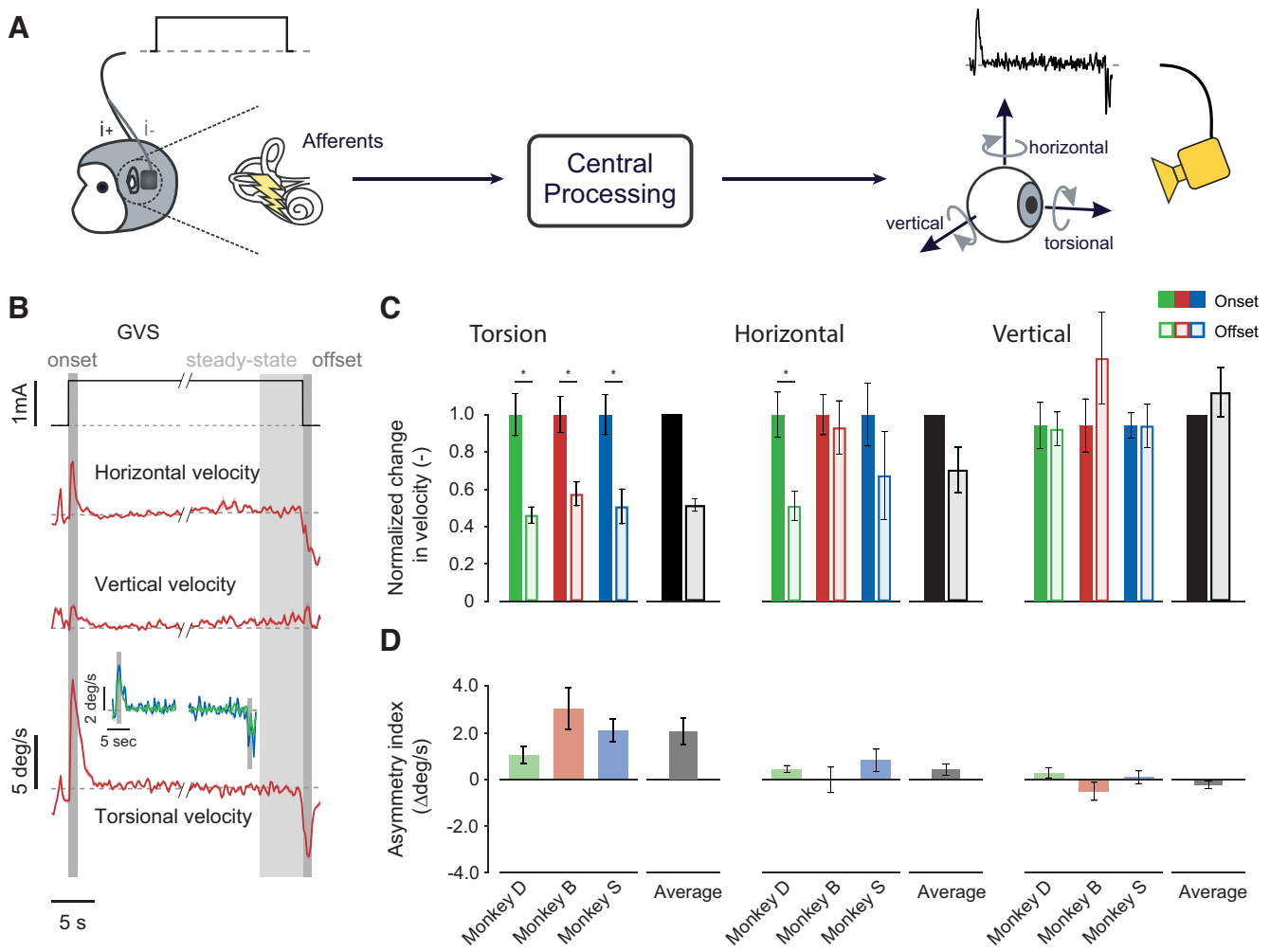

Figure 2. Constant cathodal current GVS evokes asymmetric torsional eye movements at stimulus onset versus offset. ***A***, While applying constant current GVS between surface electrodes placed on the mastoid processes, we recorded the eye movement of the animal as it was fixating on a stationary target. ***B***, Average slow phase horizontal, vertical, and torsional velocity traces at the onset, steady-state, and offset phases of the stimulation for a single animal (monkey B, red traces). Bottom trace, Asymmetric torsional eye velocities were observed at stimulus onset versus offset. Inset, The torsional velocities at stimulus onset and offset for the two other animals (monkeys D and S, green and blue). ***C***, Mean change in torsional, horizontal, and vertical eye velocity during the onset and offset phases, normalized for each monkey to the mean of the peak eye torsional, horizontal, and vertical velocity responses during the onset of the stimulus, respectively. The mean normalized change in torsional eye velocity during the offset phase was well below the onset response (i.e., 1). In contrast, the mean normalized change in horizontal and vertical eye velocity during the offset phase was similar to the onset response (i.e., 1) and only differed significantly for monkey D ($p = 0.043$). ***D***, The onset-offset asymmetry index (i.e., peak onset, peak offset) for torsional velocity was positive for all monkeys. In contrast, the onset-offset asymmetry index (i.e., peak onset minus peak offset) was close to zero for all monkeys. Error bars and shaded regions indicate the SEM. Asterisks indicate significant differences for the compared responses.

stimulation onset versus offset (asymmetry was significant in the horizontal direction for only one monkey; Fig. 2*C*). Thus, together, these results show that the activation of the vestibular nerve by the onset versus offset of cathodal GVS in awake-behaving monkeys evoked asymmetric neural responses that, in turn, produced asymmetric torsional eye movement behavior.

Cathodal GVS evokes more robust responses than anodal GVS in vestibular afferents

The onset of cathodal current stimulation produces a positive change in current flow, equivalent to that produced by the offset of anodal current stimulation. Correspondingly, an equivalent negative change in current flow is produced by the offset and onset of cathodal and anodal stimulation, respectively. Accordingly, we next predicted that consistent asymmetric afferent responses would be evoked for corresponding changes in current flow. To test this proposal, we compared the responses of afferents (irregular canal, $N = 15$; regular canal, $N = 22$; irregular otolith, $N = 12$; regular otolith, $N = 11$) to both stimuli. As shown in Figure 3, *A* and *B*, anodal stimulation evoked oppositely directed responses relative to cathodal stimulation, namely (1) an initial transient inhibitory response at the stimulation onset, (2) a subsequent steady-state response when stimulus amplitude was constant, and (3) an excitatory transient response at the stimulation offset. Further, irregular afferents were again significantly more sensitive than their regular counterparts to anodal stimulus onset and offset (Student's t tests for all phases, $p < 0.017$, Bonferroni correction for multiple comparisons). Irregular afferents displayed higher steady-state sensitivities for cathodal stimulation (Student's t tests, all p values < 0.017, Bonferroni correction for multiple comparisons), whereas no significant differences were found in the steady-state sensitivities of regular and irregular afferents for anodal stimulation (canals, $p = 0.033$; otoliths, $p = 0.054$; Bonferroni correction for multiple comparisons).

To then directly test whether GVS current steps of opposite polarity evoked asymmetric neural responses, we computed a

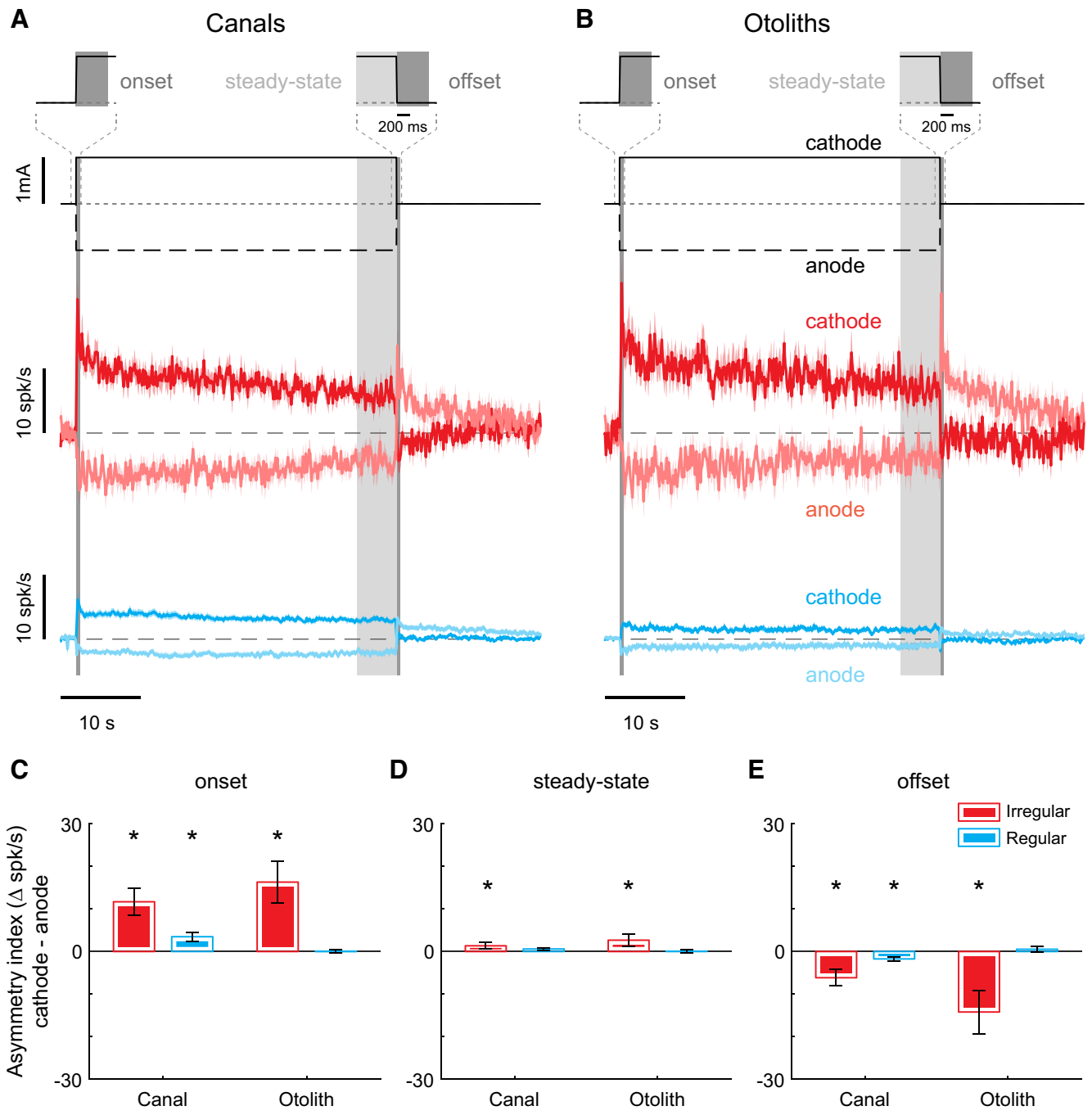

Figure 3. Constant current GVS evokes asymmetric changes in afferent firing rates during stimuli of opposing polarity. ***A***, Population averaged responses to cathodal (darker traces) and anodal (lighter traces) GVS for irregular (red) and regular (blue) canal afferents (irregular canal, $N = 15$; regular canal, $N = 22$). ***B***, Population averaged responses to cathodal (darker traces) and anodal (lighter traces) GVS for irregular (red) and regular (blue) otolith afferents (irregular otolith, $N = 12$; regular otolith, $N = 11$). ***C***, The population average cathode-anode asymmetry index of afferent firing rates during the onset phase of the stimulus showed significantly larger responses during cathode GVS (i.e., positive values) for regular and irregular canal afferents and irregular otolith afferents (Student t tests, all p values < 0.017) but not regular otolith afferents. ***D***, The population average cathode-anode asymmetry index of afferent firing rates during the steady-state phase of the stimulus showed no significant difference relative to zero for all afferent types (Student t tests, all p values > 0.017). ***E***, The population average cathode-anode asymmetry index of afferent firing rates during the offset phase of the stimulus showed significantly larger responses during anodal GVS (i.e., negative values) for regular and irregular canal afferents and irregular otolith afferents (Student t tests, all p values < 0.017) but not regular otolith afferents. Error bars and shaded regions indicate the SEM. Asterisks indicate significant differences relative to zero.

cathode-anode asymmetry index (Fig. 3*C–E*). Indeed, consistent with our initial prediction, irregular afferents displayed stronger responses to (1) the onset of cathodal versus anodal stimulation (i.e., a positive cathode-anode asymmetry index; one sample Student's t test, $p < 0.017$) and (2) the offset of anodal versus cathodal stimulation (i.e., a negative cathode-anode asymmetry index; one sample Student's t test, $p < 0.017$). Notably, afferent responses to the onset of cathodal stimulation evoked responses similar (but inverted) to the offset of anodal stimulation and vice versa. Although a comparable trend was observed for regular afferents, the overall effects of stimulation were smaller and so did not always reach significance (Fig. 3*C–E*). Thus, nonlinear

responses were evoked in irregular afferents by constant current GVS where modulation was greater for cathodal current flow.

Stochastic and sine GVS reveals primary vestibular afferent response nonlinearities

A common alternative approach for probing nonlinearities is to compare neural responses to stochastic versus single sinusoidal stimulation (Sadeghi et al., 2007b; Forbes et al., 2020). Accordingly, we also recorded afferent responses to stochastic GVS (Fig. 4*A*,*B*). To quantify the modulation of each afferent, we estimated response gains and phases and then compared these values with those estimated in response to single sinusoidal GVS across the same stimulation frequency range (0–25 Hz) as previously reported by Kwan et al. (2019). Figure 4, *C* and *D*, illustrates these results for our populations of canal (regular, blue, $N = 58$; irregular, red, $N = 48$) and otolith (regular, blue, $N = 27$; irregular, red, $N = 37$) afferents, respectively. Notably, gain and phase leads increased as a function of frequency for both regular and irregular afferents. However, the response dynamics to sinusoid and stochastic GVS deviated at low and high frequencies. Irregular canal and otolith afferents displayed higher gains at 0.2–2, and 25 Hz for stochastic versus sinusoidal GVS (Student's t test, $p < 0.0065$, Bonferroni's correction for multiple comparison). Regular canal and otolith afferents also showed similar deviations.

As shown above, irregular afferents (and regular canal afferents) display asymmetric responses to cathodal versus anodal current steps (Fig. 3). Accordingly, we predicted that a more dynamic GVS would also evoke asymmetric afferent responses. To test this proposal, we reanalyzed the vestibular afferent responses to sinusoidal GVS from Kwan et al. (2019) and separately estimated the gain for the cathodal versus anodal one-half cycles (Fig. 4*E*,*F*; see above, Materials and Methods). Consistent with our hypothesis, response gains were higher for cathodal versus anodal current in both irregular and regular canal afferents (linear mixed model, $p < 0.001$). Similarly, irregular otolith afferents showed higher response gains for cathodal current (linear mixed model, $p < 0.001$), although no significant difference was found for regular otolith afferents (linear mixed model, $p = 0.334$). We also observed a significant interaction between stimulus polarity and frequency for both irregular afferents and regular canal afferents (linear mixed model, $p < 0.001$), indicating that as frequency increased, differences observed for cathodal versus anodal current increased. Thus, together, these results provide further evidence that vestibular afferents nonlinearly encode transmastoid GVS.

Our above results establish that irregular afferents show marked nonlinearities in their responses to constant current steps (Figs. 2, 3), as well as to stochastic and sinusoidal GVS (Fig. 4). Accordingly, we fit distinct transfer functions to data obtained from the cathodal and anodal phases of stimulation (Fig. 4*E*,*F*, superimposed lines) and combined them to replicate asymmetric afferent responses to the onset and offset of cathodal and anodal stimulation (see above, Materials and Methods; Fig. 5). As expected, our nonlinear (asymmetric) fits provided a better representation of irregular afferent responses than the original linear (symmetric) fits, particularly during the offset phase (Fig. 5), whereas both fits represented the responses of our regular otolith populations, consistent with their more symmetric responses equally well (Figs. 3*C–E*, 4*E*,*F*, compare blue curves).

Motion equivalence of individual afferent firing rates and net afferent activity

Thus far, we have established that transmastoid GVS is nonlinearly (i.e., asymmetrically) encoded by vestibular afferents and that a combination of polarity-dependent transfer functions can represent this nonlinearity. These findings raise the following important question: How do these asymmetries impact the internal representation of movement that is encoded by the different afferent dynamics in response to GVS? To address this question, we inverted models of afferent response dynamics to natural motion and then estimated the equivalent virtual motion produced by GVS-evoked afferent firing rates during constant current GVS (see above, Materials and Methods; Schneider et al., 2015).

Figure 6, *A* and *B*, illustrates the time course of these estimated virtual motion signals for canal and otolith afferents, respectively. First, the virtual motion signal encoded by canal afferents comprised three main phases, (1) an initial transient, (2) a smaller linearly increasing (or decreasing) velocity (i.e., a smaller constant acceleration) throughout the stimulation, and (3) a final transient (in the opposite direction) at stimulus offset. As expected, these virtual velocity signals encoded by primary vestibular afferents demonstrated significant asymmetry for each of the three phases (Fig. 6*C–E*) characterized by larger responses (i.e., a positive cathode-anode asymmetry index) for the onset (both one-sample Student's t test, $p < 0.017$) and steady-state phases (both one-sample Student's t test, $p < 0.017$) of cathodal stimulation and larger responses for the offset phase of anodal stimulation (one-sample Student's t test, $p < 0.017$; i.e., a negative cathode-anode asymmetry index). Similarly, because of their higher GVS sensitivity, the virtual velocity signal encoded by irregular canal afferents was approximately two times larger than of their regular counterparts. Correspondingly, qualitatively similar results were obtained for otolith afferents (Fig. 6*B*) with comparable phases of virtual motion (i.e., an initial transient, a relatively constant acceleration, and a final transient), larger virtual accelerations in irregular afferents, and motion asymmetries across stimulus polarity in irregular, but not regular, afferents (Fig. 6*C–E*).

Using a combination of our mathematical modeling and single-unit recording results, we then established the time course of the GVS stimuli needed to evoke physiological sensations of a specific desired motion in the canal versus otolith systems. To do this we combined existing afferent models to natural motion (see above, Materials and Methods; Schneider et al., 2015) with our simple (inverted) nonlinear transfer functions of GVS-evoked afferent responses and computed the GVS stimulus required to generate a constant acceleration signal in each afferent type. Figure 6, *F* and *G*, shows the time course of these stimuli. Notably, to evoke a constant rotational acceleration signal in canal afferents, the required GVS stimulus is characterized by a gradual increase in current that only reaches a sustained level after ~20 s. In contrast, to evoke a constant linear acceleration signal in otolith afferents, the required GVS stimulus is characterized by a transient change in current followed by a sustained GVS level after only a few seconds.

Finally, although our above results show that asymmetrical virtual motion signals are evoked in each vestibular nerve by transmastoid GVS, our intuition was that the net signal of afferent activity evoked by binaural bipolar GVS would be symmetric across stimulus polarities because cathode-left/anode-right conditions produce the equivalent but inverted responses to anode-left/cathode-right conditions. To test this proposal, we first

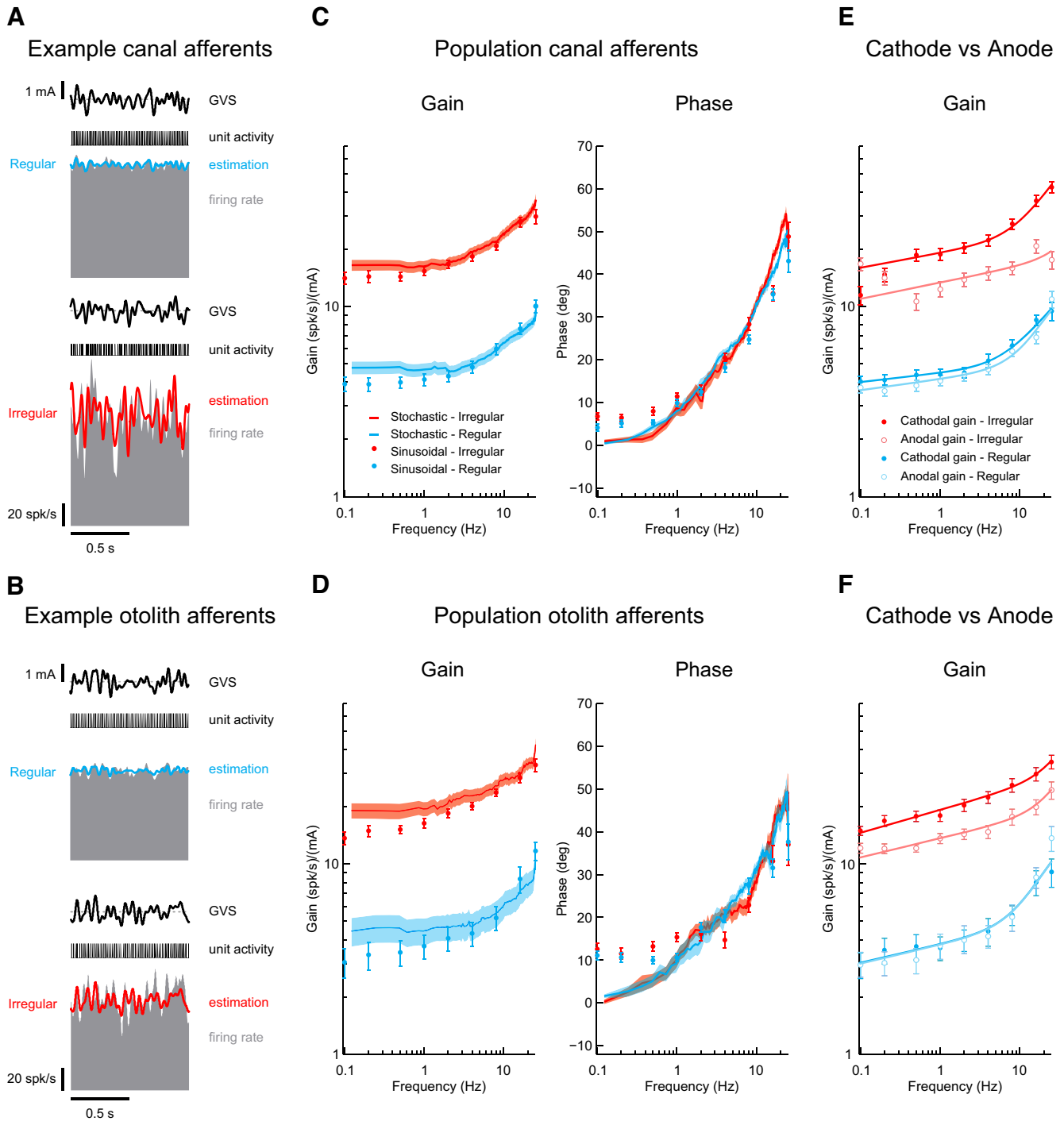

Figure 4. Vestibular afferents respond nonlinearly to stochastic and sinusoidal GVS. ***A***, ***B***, Firing rate (gray) of example regular (blue) and irregular (red) canal (***A***) and otolith (***B***) afferents to stochastic GVS. Firing rate estimates (solid blue and red lines) were found using Equation 2 and are plotted here for illustrative purposes. ***C***, Population averaged gain (left) and phase (right) of regular (blue, $N = 58$) and irregular (red, $N = 48$) canal afferents to stochastic (solid lines) and sinusoidal GVS (individual points; Kwan et al., 2019). ***D***, Population averaged gain (left) and phase (right) of regular (blue, $N = 27$) and irregular (red, $N = 37$) otolith afferents to stochastic (solid lines) and sinusoidal GVS (individual points; Kwan et al., 2019). Note the differences in gain between the two stimuli at high and low frequencies indicate nonlinear responses (***C***, ***D***). Specifically, irregular canal and otolith afferents displayed higher gains at 0.2–2, and 25 Hz for stochastic versus sinusoidal GVS. Regular canal afferents showed only deviation in gains at 0.2, 0.5, and 25 Hz, and regular otolith afferents only differ in gain at 0.2 and 0.5 Hz. ***E***, ***F***, Population averaged gains of regular (blue) and irregular (red) canal (***E***) and otolith (***F***) afferents estimated using the cathodal (filled circles) and anodal (open circles) cycles of sinusoidal GVS compared with the population averaged gain estimated from the stochastic GVS. Error bars and shaded regions indicate SEM. Model fits to the experimental data were superimposed as solid lines for each afferent type from the cathodal and anodal cycles of sinusoidal GVS. Figure 5 illustrates these fits applied to the actual irregular otolith afferent response to cathodal and anodal square wave GVS. Overall, our nonlinear (asymmetric) model provided a better fit of the data than the original linear (symmetric) model, particularly during the offset phase.

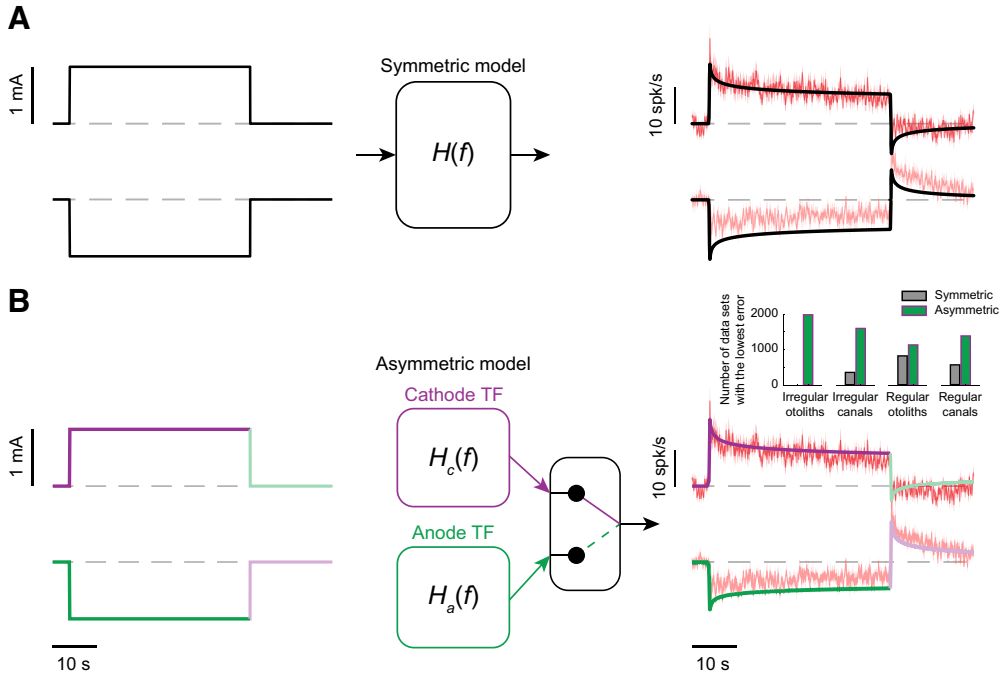

Figure 5. A nonlinear representation of afferent firing rate explains the polarity-dependent changes during constant current GVS. ***A***, A symmetric linear representation of afferent firing rates estimated from sinusoidal GVS (Kwan et al., 2019) predicted well the responses of irregular otolith afferents (red traces) to cathodal currents but poorly estimated responses to anodal currents. ***B***, An asymmetric representation of afferent firing rates combining cathodal (purple, H_c) and anodal (green, H_a) transfer functions estimated from the separate one-half cycles of sinusoidal stimulation provided a better fit to irregular otolith (red traces) afferent data. Inset top right, To quantify the ability of each model to replicate the experimental data, we computed the sum of the errors relative to the mean responses of 2000 resampled datasets. For all resampled datasets (i.e., 2000 of 2000), the asymmetric model produced a lower sum of errors for irregular canal and otolith afferents than our original linear (symmetric) model. Both models fit well the regular afferent responses (i.e., similar number of datasets with a lower error). Shaded regions on the experimental responses (red traces) indicate SEM.

simulated the signal provided by each specific semicircular canal using a 3:1 regular-to-irregular afferent weighting based on their relative distributions in the VIIIth cranial nerve (Baird et al., 1988; Goldberg, 2000). We then computed the net head motion signal from the combined semicircular afferent activity from both nerves during sinusoidal GVS (Fig. 7*A*; see above, Materials and Methods). We note that we considered semicircular canal responses only because near cancellation is predicted for the otolith end organs because of the mirrored response directions across the macula (Tribukait and Rosenhall, 2001; Fitzpatrick and Day, 2004).

In contrast to our initial prediction, we found that the net effect of stimulation provided the brain with a time-varying directional bias. Specifically, we first found that asymmetric motion signals, once projected onto Cartesian coordinates relative to Reid's plane, were provided by each canal pair, with responses in each canal that ranged from ~10 to 60% larger during cathodal versus anodal stimulation in all directions (Fig. 7*B*). The resultant virtual signal of head rotation (Fig. 7*C*) also revealed asymmetric responses; however, in the predominant directions of roll and yaw, these asymmetries were only ~2–4% larger during the cathode versus anode stimulus, indicating at least incomplete cancellation of polarity-dependent asymmetries from the separate canals. These roll and yaw asymmetries emerged primarily because the alignment of the LARP and RALP pairs were not symmetrically oriented (Della Santina et al., 2005); note, this was confirmed in simulations with symmetrically oriented canal pairs, which eliminated the net asymmetries in roll and yaw. Even more striking, motion in the pitch axis displayed a constant positive offset that occurred in both stimulus polarities and even emerged in simulations where canal pairs were oriented symmetrically. This unexpected motion signal, which was ~1% of the net signal of head rotation, arises because the pitch motion signal on the cathode side is always larger and occurs in the same direction (i.e., pitch head down) regardless of stimulus polarity. For the sake of completeness, we also performed additional simulations in which the signal provided by each specific semicircular canal was based on either only irregular or only regular afferent input. The asymmetry in pitch motion was observed in all cases, but its amplitude was sensitive to such changes in afferent weighting; exclusively irregular afferents increased asymmetry by ~2.7× (1.6°/s) and exclusively regular afferents decreased asymmetry by ~2× (0.3°/s), compared with the 3:1 ratio (0.6°/s). Overall, the polarity-dependent asymmetries in the afferent firing rates provide the brain with a time-varying directional bias in the net virtual signal of head motion that may influence perceptual/behavioral responses evoked by GVS (see below, Discussion).

Discussion

In the present study, we recorded from individual vestibular afferents in macaque monkeys to test the prevailing view that the activation of the vestibular system through GVS is inherently linear. Using a GVS setup analogous to that used in human studies, we applied external stimuli of opposing polarity and show that this view is not valid; instead, vestibular afferents encode GVS with nonlinear dynamics that differ markedly from those predicted by current models. The onset of cathodal currents produced larger changes in afferent responses compared with the onset of anodal currents, and this asymmetry was inverted during the offset of the applied currents. We observed this nonlinearity in both the semicircular and otolith systems and found

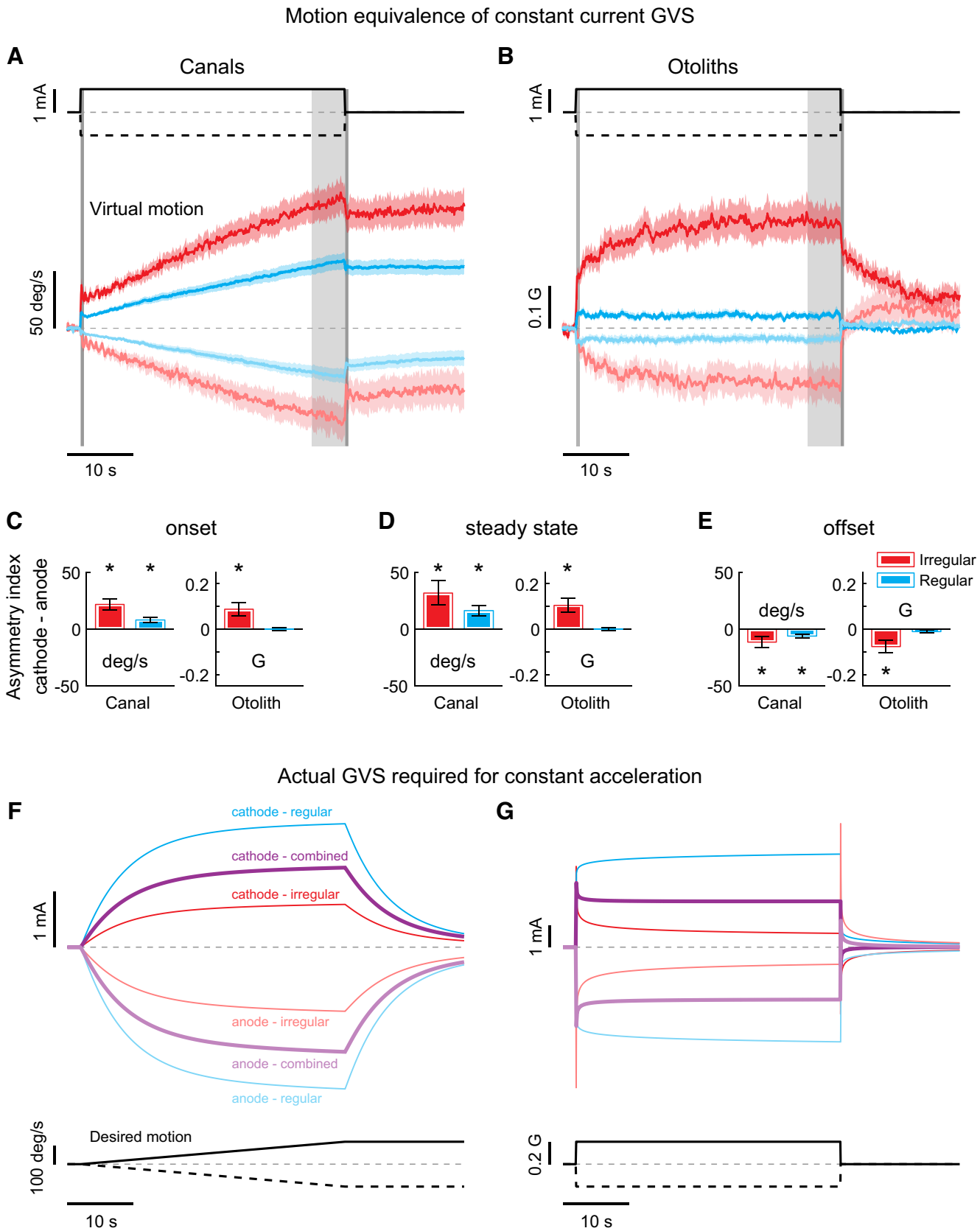

Figure 6. Semicircular canal and otolith afferent firing rates encode multiple signals of acceleration during constant current GVS. ***A***, ***B***, Population virtual motion responses to cathodal (darker traces) and anodal (lighter traces) GVS for irregular (red) and regular (blue) canal (***A***) and otolith (***B***) afferents. Virtual motion equivalent signals were estimated from the GVS-evoked afferent firing rates (Fig. 3) using inverted models of afferent responses to natural motion (Schneider et al., 2015). The horizontal dashed lines indicate zero current (top plots) and zero velocity and acceleration (bottom plots in ***A***, ***B***, respectively). ***C***, The population averaged cathode/anode asymmetry index of motion equivalent responses during the onset phase of the stimulus are significantly larger during cathode GVS for regular and irregular canal afferents and irregular otolith afferents (Student *t* tests, all *p* values < 0.017) but not regular otolith afferents. ***D***, The population averaged cathode/

that it was most marked for more irregularly discharging afferents. Using computational methods, we show that these experimentally observed nonlinear dynamics lead to an unexpected directional bias in the net population response when the information from both vestibular nerves is centrally integrated. Specifically, the observed afferent response asymmetries produce a bias in the net virtual signal of head motion to stimulation, including a polarity independent bias in the pitch direction. Whether the predicted asymmetries in the net afferent activity translate into behavioral responses in humans warrants further investigation. Thus, together our findings have important consequences for understanding how noninvasive electrical stimulation of the brain activates central neural pathways that generate perception and behavior.

Polarity dependence of vestibular afferent responses to GVS

Our results directly establish the effect of transmastoid GVS on vestibular afferent activity for cathodal versus anodal stimulation. These data contrast with those of a prior study in monkeys, which directly delivered current inside the ear and reported symmetric responses (Goldberg et al., 1984) but are consistent with previous studies in rodents that applied such internal stimulation (Kim and Curthoys, 2004; Manca et al., 2019). Interestingly, in the former case, afferents that were driven into inhibitory cutoff by anodal stimulation were excluded from analysis. Thus, given that such stimulation preferentially silences irregular afferents (for review, see Goldberg, 2000), we speculate that those afferents with the greatest asymmetries were likely excluded (Fig. 3*C–E*). Furthermore, the externally applied anodal stimulation in our present study did not completely silence any vestibular afferents. Consequently, the observed GVS-evoked response asymmetries were not limited to trivial nonlinearities such as rectification (i.e., cessation of firing). Indeed, vestibular afferents demonstrated nonlinear responses to GVS within a range of firing rates over which they display linear responses to actual motion stimuli (Sadeghi et al., 2007a; Jamali et al., 2013). Accordingly, our findings suggest that mechanical versus electrical stimulation evokes a different balance between depolarization versus hyperpolarization.

It is also noteworthy that our present results using transmastoid GVS in the monkey contrast with those reported in prior studies that applied internal stimulation in rat and mouse (Courjon et al., 1987; Manca et al., 2019). Specifically, the transmastoid GVS applied in the present study evoked a change in irregular afferent discharge that was sustained throughout the stimulus despite modest adaptation over ~10 s following the initial firing rate transient. In contrast, these previous studies reported complete adaptation that returned to baseline within 1–5 s. Thus, our present findings further demonstrate for the first time that a sustained transmastoid GVS stimulus will generate a sustained net response driven by input from all vestibular afferents from both organs. A consequence of the adaptation reported here is that for GVS pulses lasting <10 s, offset responses following both anode and cathode currents may differ from those we observed after 40 s of stimulation. To date, *in vitro* studies of the vestibular periphery have provided insight into the specific elements (e.g., channels, quantal versus nonquantal transmission, glutamate exocytosis, spike initiation, etc.) underlying electrical transduction and synaptic transmission (i.e., hair cells and afferents; Gensberger et al., 2016; Eatock, 2018). Further experimental and computational studies with varying stimulus durations will be required to establish the specific mechanisms responsible for the observed asymmetries in vestibular afferents to currents of opposite polarity. These mechanistic insights may ultimately also contribute to understanding cortical cell responses to direct current (i.e., transcranial direct current stimulation) of different polarities (Liu et al., 2018).

Motion equivalence of GVS

Our computational modeling results reveal the equivalent motion signal produced by constant current stimulation of both canal and otolith afferents. Rather than evoking a constant acceleration, this signal actually comprises the following phases: (1) an initial transient change in acceleration, (2) followed by a sustained and relatively constant signal of acceleration, and then finally (3) a transient change in acceleration in the opposite direction at stimulation offset. Consequently, only the constant acceleration signal encoded by canal afferents in response to sustained GVS supports the prevailing view that the brain interprets a galvanic signal as an angular acceleration (St George et al., 2011). Instead, we show that this relatively small constant acceleration is preceded and followed by larger transient angular accelerations for canal afferents and a change in linear acceleration for otolith afferents. Such transients in angular accelerations to GVS onset/offset were suggested by Schneider et al. (2002) but the relative magnitude of these transients were underestimated because the authors assumed that the gain and phase of afferent responses to GVS were invariant with frequency. Hence, our results have direct and quantitative implications for the design of GVS stimuli. Specifically, stimuli must differ for the specific type of afferent (i.e., regular vs irregular and canal vs otolith) to actually generate a signal of constant angular and/or linear acceleration (Fig. 6*F*,*G*). Importantly, future studies will be required to resolve how these signals are then combined by central pathways to provide a unified estimate of head motion.

Consequence of afferent asymmetry for the net signal of head motion

Our model estimating the net head motion signal combines the motion-equivalent neuronal activity across all canals, similar to Fitzpatrick and Day (2004). However, having established that GVS evokes asymmetric responses from canal afferents on each side, here we show that the net signals for each of the three rotational axes of motion will demonstrate asymmetries in response to GVS (Fig. 6). Consequently, our results overturn the generally assumed symmetrical net head rotation signals induced by GVS delivered bilaterally with currents of opposite polarity (Schneider et al., 2002; Fitzpatrick and Day, 2004; St George et al., 2011) and reveal that the pronounced neural response asymmetries evoke asymmetrical virtual net signals of head motion in all rotational directions. Our present results further make the prediction that

←

anode asymmetry index of motion equivalent responses during the steady-state phase of the stimulus were significantly larger during cathode GVS for regular and irregular canal afferents and irregular otolith afferents (Student *t* tests, all *p* values < 0.017) but not regular otolith afferents. ***E***, The population averaged cathode/anode asymmetry index of motion equivalent responses during the offset phase of the stimulus was significantly larger during anodal GVS for regular and irregular canal afferents and irregular otolith afferents (Student *t* tests, all *p* values < 0.017) but not regular otolith afferents. ***F***, ***G***, Estimated GVS signals required to evoke a signal of constant acceleration in regular (blue) and irregular (red) canal (***F***) and otolith (***G***) afferents. GVS stimuli were estimated by passing a signal of constant acceleration through motion-to-afferent firing rate models (Schneider et al., 2015) and an inverted GVS-to-afferent firing rate model established in this study. GVS stimuli assuming a combination of both afferent types were also estimated using a combined 3:1 regular-to-irregular weighting (purple). Error bars and shaded regions indicate SEM. Asterisks indicate significant differences relative to zero.

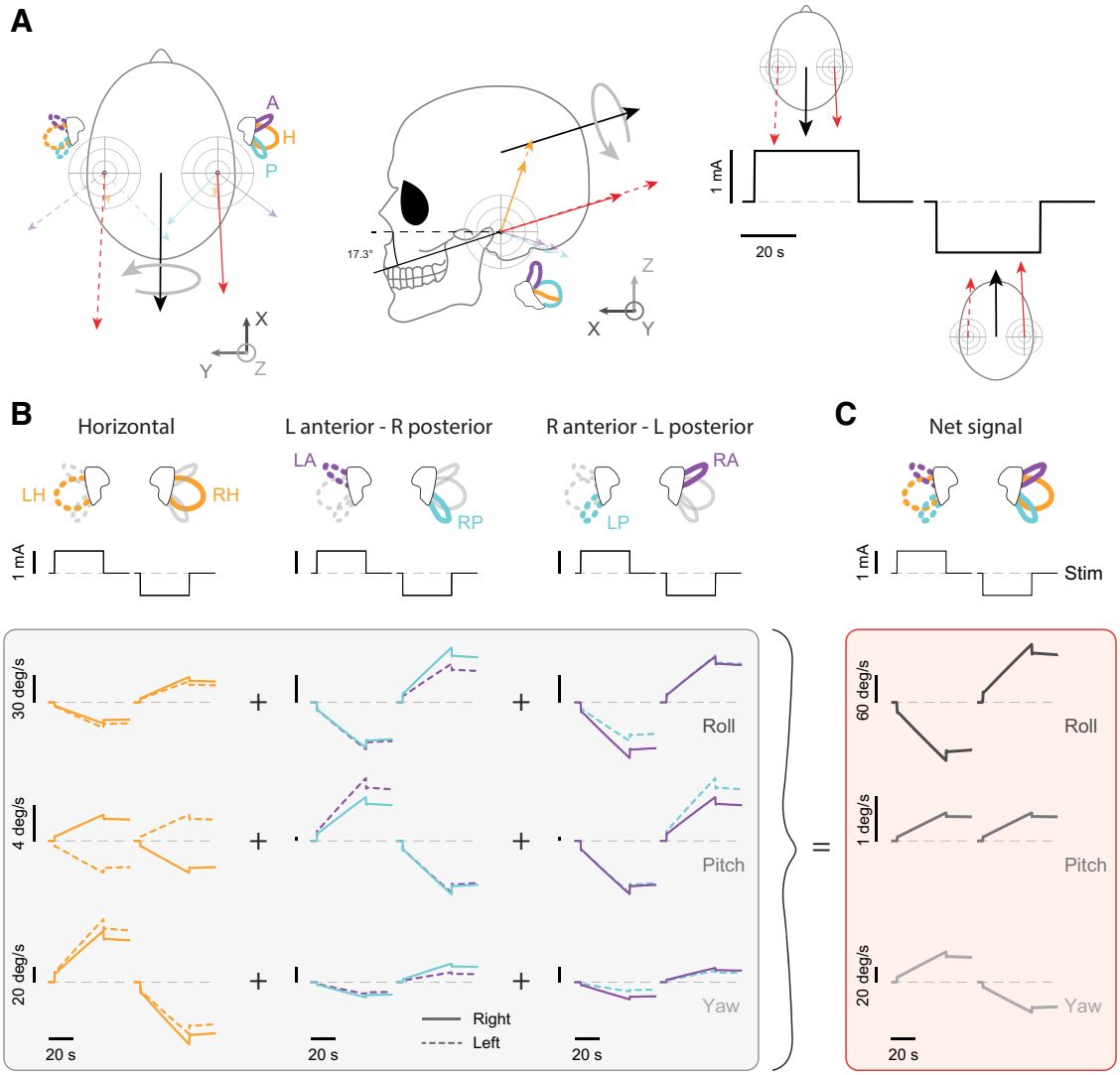

Figure 7. Asymmetric canal afferent firing produced a time-varying directional bias in the net signal of head motion during GVS applied bilaterally (with opposing polarities) over the mastoid processes. ***A***, Left, Plot shows vectors of motion equivalent semicircular canal responses to GVS (bilateral stimuli of opposite polarity) extracted from the positive peak of square wave GVS stimulation (i.e., anode right, cathode left). Vectors are oriented orthogonal to the plane of each canal (A, anterior; H, horizontal; P, posterior) on the left (L) and right (R) side of the head using the canal orientations reported by Della Santina et al. (2005); the resultant vectors for each labyrinth (i.e., left and right) are shown as red arrows. The vector average of the resultants from both sides is depicted as a large black arrow, and the gray curved arrow shows the direction of rotation. Right, Plot shows the net vector representations plotted at the positive (i.e., anode right) and negative (i.e., cathode right) peaks of the stimulus cycle and depicts the asymmetry of the responses arising from the left and right labyrinths. The coordinate system (X-, Y-, and Z-axes) show the Cartesian coordinates aligned with the Reid's stereotactic line. ***B***, For each canal pair (horizontal, left anterior (LA) - right posterior (RP) and right anterior (RA) - left posterior (LP)), time-varying signals of motion estimated in response to GVS were projected onto Cartesian coordinates (*X*, *Y*, and *Z*) to provide rotational velocities in roll, pitch, and yaw directions (i.e., the 3 rows in the gray shaded regions). Furthermore, for each canal pair and in most directions (i.e., roll, pitch and yaw), larger velocities were observed in the canal that was activated by the cathodal current (i.e., the right canal during positive GVS and vice versa during negative GVS). Note, the magnitude of the asymmetries within each canal pair (and their net effects) depends on their orientation of each canal relative to the roll, pitch, and yaw axes (Della Santina et al., 2005). ***C***, The net signal of head motion in the roll, pitch, and yaw directions from the summation of all canal pairs (i.e., the 3 rows in the red shaded region). Notably, in the pitch direction (middle row), afferent asymmetries manifested as a small (<1°/s) net velocity signal in a positive direction (i.e., nose down rotation or flexion) for both the cathodal and anodal stimulus conditions. The amplitude of the pitch asymmetry was also sensitive to such changes in afferent weighting with exclusively irregular versus regular afferents input exacerbating or diminishing this asymmetry, respectively.

square wave GVS evokes a net pitch motion signal that maintains a directionally constant offset regardless of stimulus polarity (Fig. 6*C*). This pitch bias arises because the pitch component of the net motion signal is always larger on the cathode side and occurs in the same direction (i.e., pitch head down) for both stimulus polarities (i.e., cathode-left/anode-right versus anode-left/cathode-right). Although the magnitude of this pitch asymmetry is only ~1% of the net vector of motion, we posit that the magnitude of this response can be further modified by the relative alignment of canals within each pair. For example, based on the canal orientations reported by Della Santina et al. (2005), our model predicts that misalignment of canals pairs within a physiologically plausible range (i.e., 95% confidence intervals) could theoretically increase the pitch signal to 4% of the net vector of motion or even invert this signal to produce a negative offset.

Behavioral correlates of constant current GVS-evoked vestibular afferent responses

Our above results raise the question of whether the GVS-evoked afferent responses and related asymmetries in predicted net head motion signals are reflected in evoked behaviors. Indeed, there is evidence that this is the case. For example, the three phases of afferent responses (i.e., onset, steady-state, and offset) are consistent with the time course of whole-body balance responses

evoked in humans by comparable GVS applied to the mastoid processes, an initial and rapid change in tilt position toward the anode at GVS onset, followed by a slower movement that lasts ~6 s, ending with a fast whole-body movement in the opposite direction at GVS offset (Inglis et al., 1995; Day et al., 1997; Wardman et al., 2003a). Furthermore, eye movement asymmetries similar to those described in our nonhuman primate-based model have been reported for humans (MacDougall et al., 2003; Jahn et al., 2003b), although MacDougall et al. (2003) concluded that eye movement amplitudes were comparable for stimuli of opposing polarity. Nevertheless, researchers generally assume symmetry in vestibular activation by cathodal and anodal currents and often combine responses to both polarities (Day et al., 1997; Cathers et al., 2005; Mian and Day, 2014; Fitzpatrick and Watson, 2015; Mackenzie and Reynolds, 2018).

Finally, our results have important implications for the implementation of GVS in clinical and research applications. First, our findings clearly establish that assessments of vestibular function requiring unilateral electrical stimuli need to consider asymmetrical activation of vestibular afferents to currents of opposite polarity. Second, our findings can be leveraged to improve our mechanistic understanding of asymmetric afferent activation on vestibular function in humans. For example, distinct net response asymmetries can be manipulated by controlling the polarity of bilateral current application to each mastoid process (Day et al., 2010). Indeed, our model of net afferent activity evoked by GVS applied bilaterally with the same polarity predicts a 30% increase in the magnitude of pitch rotation for cathodal versus anodal stimuli, compared with the 1–4% asymmetries predicted for bilateral application of currents with opposite polarity. Thus, experiments focusing on precise behavioral measures will be required to confirm the asymmetric predictions arising from our model. A potential confound, however, is that the current from each unilateral stimulus path may spread to the contralateral vestibular organ (Aw et al., 2013; Woo et al., 2019). Hence, further investigations are also required to determine how vestibular afferents respond to GVS stimulation delivered to the contralateral mastoid process. Finally, it may be also possible to identify how different combinations of regular and irregular afferents contribute to vestibular-evoked response. For example, predictions from our model show that the amplitude of asymmetries identified in the pitch direction are sensitive to the afferent weighting, with exclusively irregular versus regular afferents input exacerbating or diminishing this asymmetry, respectively. This suggests that modeling distinct regular-to-irregular afferent ratios may be needed to predict the asymmetric input for different vestibulomotor systems and that asymmetric behaviors may be best identified through vestibular pathways that favor irregular afferents (vestibulospinal reflexes), as opposed to those that favor regular afferents (i.e., vestibulo-ocular reflexes; Cullen, 2019).

References

Angelaki DE, Dickman JD (2000) Spatiotemporal processing of linear acceleration: primary afferent and central vestibular neuron responses. J Neurophysiol 84:2113–2132.

Aw ST, Todd MJ, Lehnen N, Aw GE, Weber KP, Eggert T, Halmagyi GM (2013) Electrical vestibular stimulation after vestibular deafferentation and in vestibular schwannoma. PLoS One 8:e82078.

Baird RA, Desmadryl G, Fernández C, Goldberg JM (1988) The vestibular nerve of the chinchilla. II. Relation between afferent response properties and peripheral innervation patterns in the semicircular canals. J Neurophysiol 60:182–203.

Bent LR, Inglis JT, McFadyen BJ (2004) When is vestibular information important during walking? J Neurophysiol 92:1269–1275.

Britton TC, Day BL, Brown P, Rothwell JC, Thompson PD, Marsden CD (1993) Postural electromyographic responses in the arm and leg following galvanic vestibular stimulation in man. Exp Brain Res 94:143–151.

Bunn LM, Marsden JF, Voyce DC, Giunti P, Day BL (2015) Sensorimotor processing for balance in spinocerebellar ataxia type 6. Mov Disord 30:1259–1266.

Cathers I, Day BL, Fitzpatrick RC (2005) Otolith and canal reflexes in human standing. J Physiol 563:229–234.

Chen A, Khosravi-Hashemi N, Kuo C, Kramer JK, Blouin JS (2019) Development of a conversion model between mechanical and electrical vestibular stimuli. J Neurophysiol 123:548–559.

Chen A, Kuo C, Blouin JS (2022) A portable and low-cost solution for real-time manipulation of the vestibular sense. Journal of Neuroscience Methods 382:109709.

Chiarovano E, de Waele C, MacDougall HG, Rogers SJ, Burgess AM, Curthoys IS (2015) Maintaining balance when looking at a virtual reality three-dimensional display of a field of moving dots or at a virtual reality scene. Front Neurol 6:164.

Courjon JH, Precht W, Sirkin DW (1987) Vestibular nerve and nuclei unit responses and eye movement responses to repetitive galvanic stimulation of the labyrinth in the rat. Exp Brain Res 66:41–48.

Cullen KE (2019) Vestibular processing during natural self-motion: implications for perception and action. Nat Rev Neurosci 20:346–363.

Dale A, Cullen KE (2013) The nucleus prepositus predominantly outputs eye movement-related information during passive and active self-motion. J Neurophysiol 109:1900–1911.

Dale A, Cullen KE (2015) Local population synchrony and the encoding of eye position in the primate neural integrator. J Neurosci 35:4287–4295.

Day BL, Cauquil AS, Bartolomei L, Pastor MA, Lyon IN (1997) Human body-segment tilts induced by galvanic stimulation: a vestibularly driven balance protection mechanism. J Physiol 500:661–672.

Day BL, Marsden JF, Ramsay E, Mian OS, Fitzpatrick RC (2010) Non-linear vector summation of left and right vestibular signals for human balance. J Physiol 588:671–682.

Della Santina CC, Potyagaylo V, Migliaccio AA, Minor LB, Carey JP (2005) Orientation of human semicircular canals measured by three-dimensional multiplanar CT reconstruction. J Assoc Res Otolaryngol 6:191–206.

Dietrich H, Heidger F, Schniepp R, MacNeilage PR, Glasauer S, Wuehr M (2020) Head motion predictability explains activity-dependent suppression of vestibular balance control. Sci Rep 10:668.

Dlugaiczyk J, Gensberger KD, Straka H (2019) Galvanic vestibular stimulation: from basic concepts to clinical applications. J Neurophysiol 121:2237–2255.

Eatock RA (2018) Specializations for fast signaling in the amniote vestibular inner ear. Integr Comp Biol 58:341–350.

Fitzpatrick RC, Day BL (2004) Probing the human vestibular system with galvanic stimulation. J Appl Physiol (1985) 96:2301–2316.

Fitzpatrick RC, Watson SR (2015) Passive motion reduces vestibular balance and perceptual responses. J Physiol 593:2389–2398.

Fitzpatrick RC, Butler JE, Day BL (2006) Resolving head rotation for human bipedalism. Curr Biol 16:1509–1514.

Forbes PA, Siegmund GP, Schouten AC, Blouin JS (2015) Task, muscle and frequency dependent vestibular control of posture. Front Integr Neurosci 8:94.

Forbes PA, Luu BL, Van der Loos HF, Croft EA, Inglis JT, Blouin JS (2016) Transformation of vestibular signals for the control of standing in humans. J Neurosci 36:11510–11520.

Forbes PA, Vlutters M, Dakin CJ, van der Kooij H, Blouin JS, Schouten AC (2017) Rapid limb-specific modulation of vestibular contributions to ankle muscle activity during locomotion. J Physiol 595:2175–2195.

Forbes PA, Kwan A, Rasman BG, Mitchell DE, Cullen KE, Blouin JS (2020) Neural mechanisms underlying high-frequency vestibulocollic reflexes in humans and monkeys. J Neurosci 40:1874–1887.

Gensberger KD, Kaufmann AK, Dietrich H, Branoner F, Banchi R, Chagnaud BP, Straka H (2016) Galvanic vestibular stimulation: cellular substrates and response patterns of neurons in the vestibulo-ocular network. J Neurosci 36:9097–9110.

Goldberg JM (2000) Afferent diversity and the organization of central vestibular pathways. Exp Brain Res 130:277–297.

Goldberg JM, Smith CE, Fernández C (1984) Relation between discharge regularity and responses to externally applied galvanic currents in vestibular nerve afferents of the squirrel-monkey. J Neurophysiol 51:1236–1256.

Goldberg JM, Wilson VJ, Cullen KE, Angelaki DE, Broussard DM, Buttner-Ennever JA, Fukushima K, Minor LB (2012) The vestibular system: a sixth sense. New York: Oxford UP.

Hays AVJ, Richmond BJ, Optican LM (1982) Unix-based multiple-process system, for real-time data acquisition and control. El Segundo, CA: Electron Conventions.

Hullar TE, Della Santina CC, Hirvonen T, Lasker DM, Carey JP, Minor LB (2005) Responses of irregularly discharging chinchilla semicircular canal vestibular-nerve afferents during high-frequency head rotations. J Neurophysiol 93:2777–2786.

Inglis JT, Shupert CL, Hlavacka F, Horak FB (1995) Effect of galvanic vestibular stimulation on human postural responses during support surface translations. J Neurophysiol 73:896–901.

Jahn K, Naessl A, Schneider E, Strupp M, Brandt T, Dieterich M (2003a) Inverse U-shaped curve for age dependency of torsional eye movement responses to galvanic vestibular stimulation. Brain 126:1579–1589.

Jahn K, Naessl A, Strupp M, Schneider E, Brandt T, Dieterich M (2003b) Torsional eye movement responses to monaural and binaural galvanic vestibular stimulation: side-to-side asymmetries. Ann N Y Acad Sci 1004:485–489.

Jamali M, Carriot J, Chacron MJ, Cullen KE (2013) Strong correlations between sensitivity and variability give rise to constant discrimination thresholds across the otolith afferent population. J Neurosci 33:11302–11313.

Jarvis MR, Mitra PP (2001) Sampling properties of the spectrum and coherency of sequences of action potentials. Neural Comput 13:717–749.

Khosravi-Hashemi N, Forbes PA, Dakin CJ, Blouin JS (2019) Virtual signals of head rotation induce gravity-dependent inferences of linear acceleration. J Physiol 597:5231–5246.

Kim HJ, Choi JY, Son EJ, Lee WS (2006) Response to galvanic vestibular stimulation in patients with unilateral vestibular loss. Laryngoscope 116:62–66.

Kim J, Curthoys IS (2004) Responses of primary vestibular neurons to galvanic vestibular stimulation (GVS) in the anaesthetised guinea pig. Brain Res Bull 64:265–271.

Kwan A, Forbes PA, Mitchell DE, Blouin J-S, Cullen KE (2019) Neural substrates, dynamics and thresholds of galvanic vestibular stimulation in the behaving primate. Nat Commun 10:1904.

Liu A, Vöröslakos M, Kronberg G, Henin S, Krause MR, Huang Y, Opitz A, Mehta A, Pack CC, Krekelberg B, Berényi A, Parra LC, Melloni L, Devinsky O, Buzsáki G (2018) Immediate neurophysiological effects of transcranial electrical stimulation. Nat Commun 9:5092.

MacDougall HG, Brizuela AE, Curthoys IS (2003) Linearity, symmetry and additivity of the human eye-movement response to maintained unilateral and bilateral surface galvanic (DC) vestibular stimulation. Exp Brain Res 148:166–175.

Mackenzie SW, Reynolds RF (2018) Differential effects of vision upon the accuracy and precision of vestibular-evoked balance responses. J Physiol 596:2173–2184.

Magnani RM, Bruijn SM, van Dieën JH, Forbes PA (2021) Stabilization demands of walking modulate the vestibular contributions to gait. Sci Rep 11:13736.

Manca M, Glowatzki E, Roberts DC, Fridman GY, Aplin FP (2019) Ionic direct current modulation evokes spike-rate adaptation in the vestibular periphery. Sci Rep 9:18924.

Massot C, Chacron MJ, Cullen KE (2011) Information transmission and detection thresholds in the vestibular nuclei: single neurons vs. population encoding. J Neurophysiol 105:1798–1814.

Mian OS, Day BL (2009) Determining the direction of vestibular-evoked balance responses using stochastic vestibular stimulation. J Physiol 587:2869–2873.

Mian OS, Day BL (2014) Violation of the craniocentricity principle for vestibularly evoked balance responses under conditions of anisotropic stability. J Neurosci 34:7696–7703.

Nashner LM, Wolfson P (1974) Influence of head position and proprioceptive cues on short latency postural reflexes evoked by galvanic stimulation of human labyrinth. Brain Res 67:255–268.

Paulin MG (1992) Digital filters for firing rate estimation. Biol Cybern 66:525–531.

Ramachandran R, Lisberger SG (2006) Transformation of vestibular signals into motor commands in the vestibuloocular reflex pathways of monkeys. J Neurophysiol 96:1061–1074.

Richmond BJ, Optican LM (1990) Temporal encoding of two-dimensional patterns by single units in primate primary visual cortex. II. Information transmission. J Neurophysiol 64:370–380.

Sadeghi SG, Chacron MJ, Taylor MC, Cullen KE (2007a) Neural variability, detection thresholds, and information transmission in the vestibular system. J Neurosci 27:771–781.

Sadeghi SG, Minor LB, Cullen KE (2007b) Response of vestibular-nerve afferents to active and passive rotations under normal conditions and after unilateral labyrinthectomy. J Neurophysiol 97:1503–1514.

Sadeghi SG, Goldberg JM, Minor LB, Cullen KE (2009) Efferent-mediated responses in vestibular nerve afferents of the alert macaque. J Neurophysiol 101:988–1001.

Schneider AD, Jamali M, Carriot J, Chacron MJ, Cullen KE (2015) The increased sensitivity of irregular peripheral canal and otolith vestibular afferents optimizes their encoding of natural stimuli. J Neurosci 35:5522–5536.

Schneider E, Glasauer S, Dieterich M (2002) Comparison of human ocular torsion patterns during natural and galvanic vestibular stimulation. J Neurophysiol 87:2064–2073.

Schniepp R, Boerner JC, Decker J, Jahn K, Brandt T, Wuehr M (2018) Noisy vestibular stimulation improves vestibulospinal function in patients with bilateral vestibulopathy. J Neurol 265:57–62.

St George RJ, Day BL, Fitzpatrick RC (2011) Adaptation of vestibular signals for self-motion perception. J Physiol 589:843–853.

Tribukait A, Rosenhall U (2001) Directional sensitivity of the human macula utriculi based on morphological characteristics. Audiol Neurootol 6:98–107.

Wardman DL, Day BL, Fitzpatrick RC (2003a) Position and velocity responses to galvanic vestibular stimulation in human subjects during standing. J Physiol 547:293–299.

Wardman DL, Taylor JL, Fitzpatrick RC (2003b) Effects of galvanic vestibular stimulation on human posture and perception while standing. J Physiol 551:1033–1042.

Watson SRD, Brizuela AE, Curthoys IS, Colebatch JG, MacDougall HG, Halmagyi GM (1998) Maintained ocular torsion produced by bilateral and unilateral galvanic (DC) vestibular stimulation in humans. Exp Brain Res 122:453–458.

Woll J, Sprenger A, Helmchen C (2019) Postural control during galvanic vestibular stimulation in patients with persistent perceptual-postural dizziness. J Neurol 266:1236–1249.

Woo EJ, Siegmund GP, Reilly CW, Blouin JS (2019) Asymmetric unilateral vestibular perception in adolescents with idiopathic scoliosis. Front Neurol 10:1270.

Zink R, Bucher SF, Weiss A, Brandt T, Dieterich M (1998) Effects of galvanic vestibular stimulation on otolithic and semicircular canal eye movements and perceived vertical. Electroencephalogr Clin Neurophysiol 107:200–205.